

Section 2

ADVANCED TECHNOLOGY DEVELOPMENTS

2.A Observation of Gain on XUV Transitions in Ne-like and Li-like Ions

Population inversion and amplified spontaneous emission (ASE) at soft x-ray wavelengths have been achieved using two methods of pumping: collisional and recombinational. In the collisionally excited x-ray laser, thermal electrons in the plasma excite ions to the upper laser state, which is a forbidden radiative transition to the ground state but is easily excited by collisions and dielectronic recombinations. Population therefore accumulates in the upper state while the lower laser level is depopulated by a rapid radiative transition rate. The first collisionally pumped laser was demonstrated by Lawrence Livermore National Laboratory (LLNL)¹ in Ne-like Se and has been extensively studied in various other elements and extended to several Ni-like species.² These experiments use thin exploding-foil targets to ensure that refraction effects are minimized. The pump laser burns through the target foil near the peak of the pulse, causing the foil to explode symmetrically. The resulting density profile is relatively flat in the central region and falls off in both directions along the incident laser axis. This allows x rays to propagate along the axis of the plasma and be significantly amplified before leaving the plasma.

Collisionally excited x-ray lasing can also be produced using slab targets.³ In this case, the target thickness is such that the pump laser does not burn through the target during the pulse. This gives rise to a steep density gradient in the direction of the incident laser because the target mass is not depleted and a region of solid density persists for the duration of the laser

pulse. Since there is no axis of symmetry in the density profile, all rays suffer refraction away from the target. This behavior was originally thought to be a severe detriment to the attainment of gain. The results of Ref. 3 are thus unexpected and merit further study.

We have carried out experiments that utilize slab targets and produce lasing in Ne-like Ge, using lower laser energy than in previous experiments. The wavelengths of the five lasing lines range from 196 Å to 287 Å. We will show the scaling of the laser output with target length and present measurements of the divergence of this x-ray laser.

In a recombination-pumped laser the mean ionization of the plasma is higher than that of an equilibrium plasma at the same temperature. In this nonequilibrium condition, which occurs following a rapid cooling, three-body recombination and radiative cascading dominate over collisional ionization and excitation processes. This tends to populate the upper levels (e.g., $4f$ and $5f$ in Li-like ions) more than the lower excited states, thus creating an inversion. Furthermore, the lower level ($3d$) has a short lifetime because of a strong radiative transition to the ground state.⁴

This nonequilibrium situation is typically created by heating the plasma with a short laser pulse and then allowing it to cool in a time that is short compared to the recombination time for the ions involved. Since the recombination time for ions of interest (i.e., lasing at wavelengths <200 Å) is of the order of tens of picoseconds, these types of experiments usually require laser pulses shorter than 100 ps. Such experiments have produced various types of recombination lasing.⁵ In long-pulse experiments, any lasing occurs while the pump laser is heating the plasma; therefore, it must occur far from the target surface where the plasma absorbs very little laser energy and is thus able to cool quickly. At this point, collisional excitation and ionization (dominant in the region heated by the laser) are insignificant compared to recombination.

Recent results by Hara *et al.*⁶ have shown that the intensity of the $3d-4f$ and $3d-5f$ lines of Li-like Al increases exponentially with length in experiments using very-low-power, 5-ns laser pulses. We present results of experiments with Li-like Al performed at somewhat higher intensities than reported in Ref. 6 and show apparent ASE of the lines at 105 Å and 154 Å. We also present results that extend the Li-like scheme to shorter wavelengths, i.e., a Li-like Ti transition at 47 Å. The Ti experiments also showed a lasing line at 326.5 Å that has been tentatively identified as transition in Ne-like Ti.⁷ Finally, we present angular-distribution measurements of the output of these x-ray lasers.

Experimental Configuration

At LLE experiments were performed using the glass development laser (GDL).⁸ The targets were irradiated with 650-ps pulses of 1054-nm light at various intensities. The line focus was produced by the addition of a cylindrical corrector lens to the $f/3$ spherical focus lens normally used in

laser-plasma interaction experiments. To produce sufficient excitation of the $3p$ state in the Ne-like Ge ion (of excitation energy 1480 eV), a temperature in the range of 600 eV–1000 eV is required. Such temperatures are produced using on-target intensities of $\sim 2 \times 10^{13} \text{ W/cm}^2$ as evidenced by the observation of Ne-like lines in the x-ray and XUV spectra.

A grazing incidence grating spectrometer (GIGS) is used to view the plasma end-on to detect the output of the x-ray laser, as shown in Fig. 42.12. The spectrometer has an acceptance angle of $\sim 20 \text{ mrad}$ in the direction along the entrance slit and a focusing mirror provides a collection angle of $\sim 1 \text{ mrad}$ perpendicular to the slit. A crystal spectrometer and an x-ray pinhole camera are used to measure the x-ray spectrum and the intensity distribution of the optical laser at line focus, respectively. All diagnostics are time integrated and use film for recording. Kodak 2497 film is used in the pinhole and crystal spectrometer; Kodak 101 film is used in the GIGS. An advantage of using film in the GIGS rather than three narrow strips of microchannel plate as used in Refs. 1 and 2 is that a more complete record of the angular output intensity perpendicular to the dispersion direction is obtained on film.

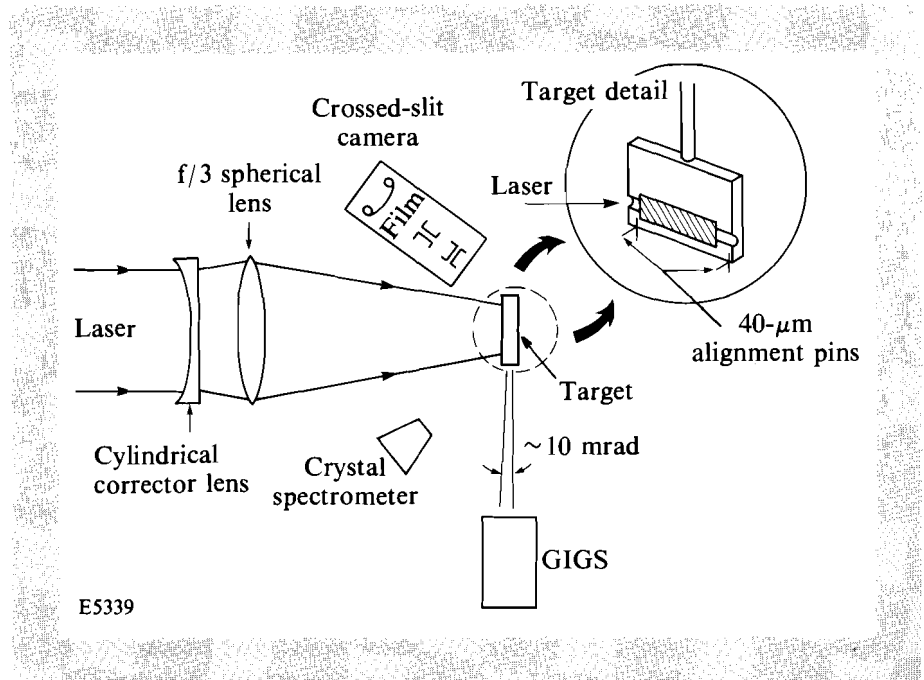


Fig. 42.12

The experimental configuration for x-ray laser experiments on GDL. The insert depicts an x-ray laser target with glass-fiber alignment pins.

Gain measurements are performed by comparing the output intensity from targets of different length. The target length is varied by using different target slab lengths while maintaining the laser line-focus length. This ensures that variations caused by laser irradiance differences are kept to a minimum since the targets sample only the central region of the beam. For example, the longest targets (22 mm) are overfilled by the line focus

by ~2 mm. The x-ray and XUV film densities are converted to intensity using x-ray calibration data.⁹ The reflectivity of the grating and collection mirror has not been absolutely calibrated; all intensities are therefore in relative units.

Results

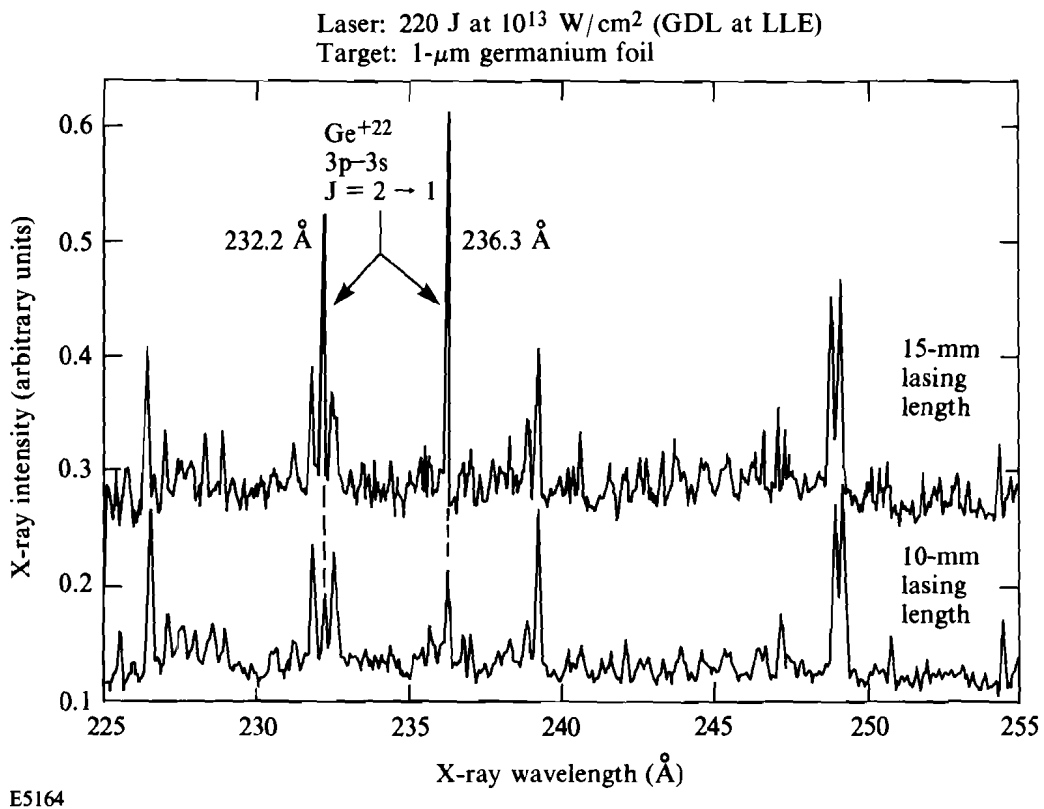
1. Ne-like germanium

The Ge targets consist of 125- μm Mylar foil coated with $\geq 1\text{-}\mu\text{m}$ GE thickness, which is much larger than the heat-front penetration depth. The Mylar backing serves to provide a resilient support ensuring the flatness of the Ge surface. Segments of 40- μm glass fibers are used as alignment reference pins to be imaged in the target alignment microscope as shown in the inset of Fig. 42.12. Using these pins and the edge of the target enables us to align the target, spectrometer, and line-focus axes to better than 5-mrad accuracy.

Fig. 42.13

A comparison of the output intensity of the $J=2-1$ Ge^{+22} lines (232 Å and 236 Å) for two x-ray laser lengths. The lower spectrum is for a 10-mm plasma length and the upper spectrum is for a 15-mm length.

The presence of gain and the effect of laser length on x-ray laser output are demonstrated in Figs. 42.13 and 42.14. Figure 42.13 shows similar regions of the XUV spectra (from GIGS) from two different target lengths. Both spectra are shown after conversion to relative intensity. Note that for the 10-mm-long targets the lasing lines are barely discernible ($J=2 \rightarrow 1$



at 232 Å and 236 Å), whereas for the 15-mm length the lines begin to be the dominant features in the spectrum. For line foci shorter than 10 mm, the lasing lines could hardly be seen.

If the line focus is extended to 22 mm, the lasing lines become the brightest lines in the spectrum. Figure 42.14 shows the Ge spectrum (from GIGS) in the range of ~20 Å–380 Å from a 22-mm-long target irradiated at an intensity of 1.5×10^{13} W/cm². The lasing lines of Ne-like Ge are labeled (a) to (e) and correspond to the designation in Table 42.I. The nonlasing lines have approximately the same intensity as those in the shots of Fig. 42.13. The carbon *K* absorption edge can be seen at 43.6 Å and results from the carbon in the film emulsion and impurity coatings on the GIGS optics.

Fig. 42.14

A wide range of the spectrum from a 22-mm-long Ge x-ray laser target. The lines designated (a) – (e) are the various 3*p*–3*s* lasing lines observed in Ne-like Ge.

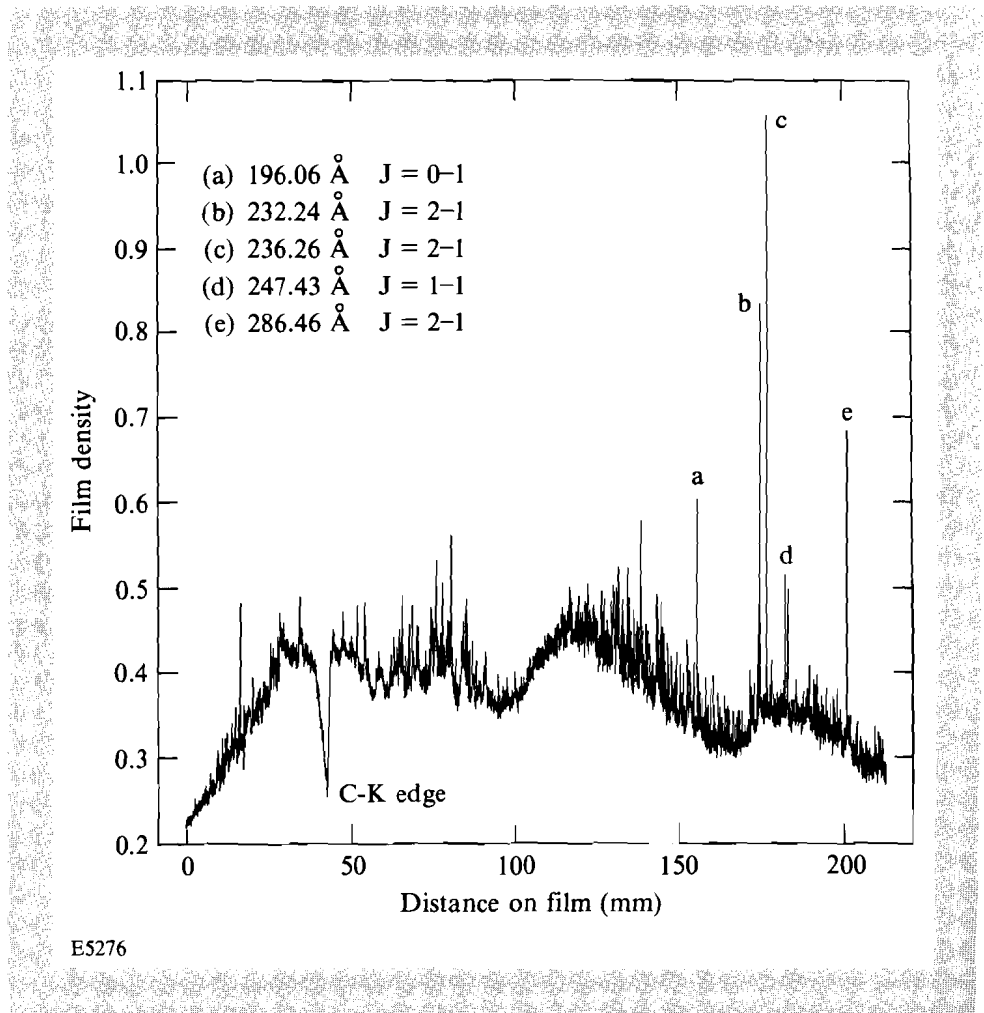


Figure 42.15 is a plot of the relative intensity I of the $J = 2-1$ lasing line at 236 Å as a function of the Ge target length ℓ . The data points are obtained from different shots that had nominally the same optical laser conditions ($\pm 10\%$). The solid curve is a best fit of the analytic expression

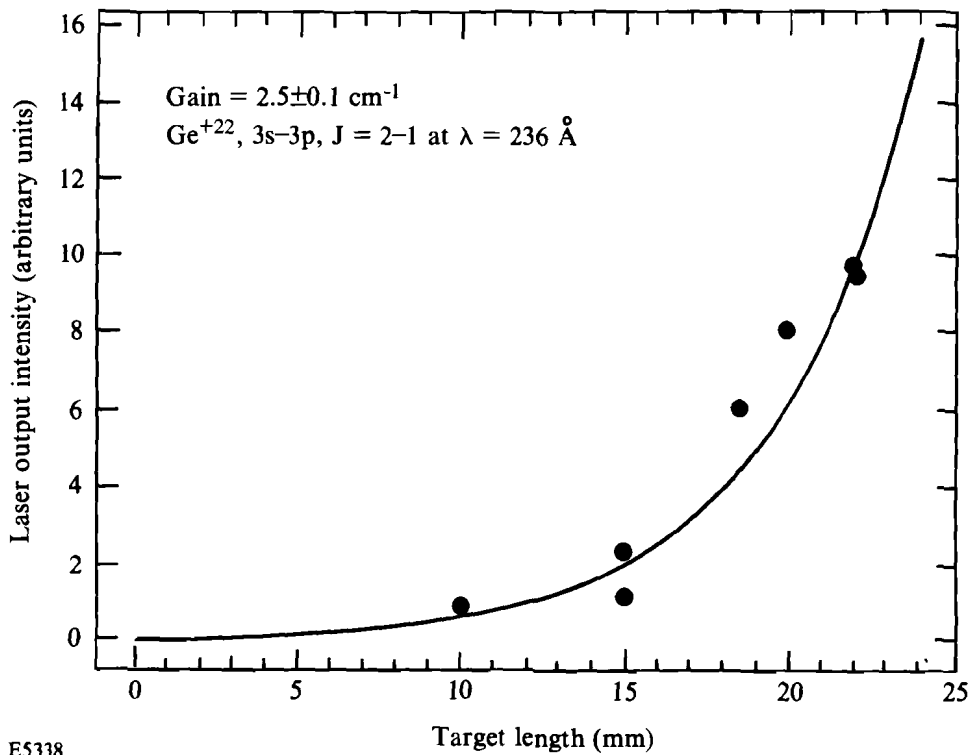
$$I \propto [\exp(g\ell) - 1]^{3/2} / [(g\ell)\exp(g\ell)]^{1/2} \quad (1)$$

to the data. From this we derive the gain coefficient g . This method was likewise applied to the other lasing lines. The resulting gains are shown in Table 42.I.

Table 42.I: Lasing lines and their designations.

Designation	Transition	Wavelength (\AA)	Gain (cm^{-1})
(a)	$(2p^5_{1/2}3p_{1/2})_0 - (2p^5_{1/2}3s_{1/2})_1$	196.06	1.5
(b)	$(2p^5_{3/2}3p_{3/2})_2 - (2p^5_{3/2}3s_{1/2})_1$	232.24	2.5
(c)	$(2p^5_{1/2}3p_{3/2})_2 - (2p^5_{1/2}3s_{1/2})_1$	236.26	2.5
(d)	$(2p^5_{3/2}3p_{3/2})_1 - (2p^5_{3/2}3s_{1/2})_1$	247.32	1.0
(e)	$(2p^5_{3/2}3p_{1/2})_2 - (2p^5_{3/2}3s_{1/2})_1$	286.46	1.8

E5593



E5338

Fig. 42.15 Intensity of the 236- \AA line of Ge^{+22} versus target length. The gain is obtained from the solid curve, which is a fit of Eq. (1) to the experimental points.

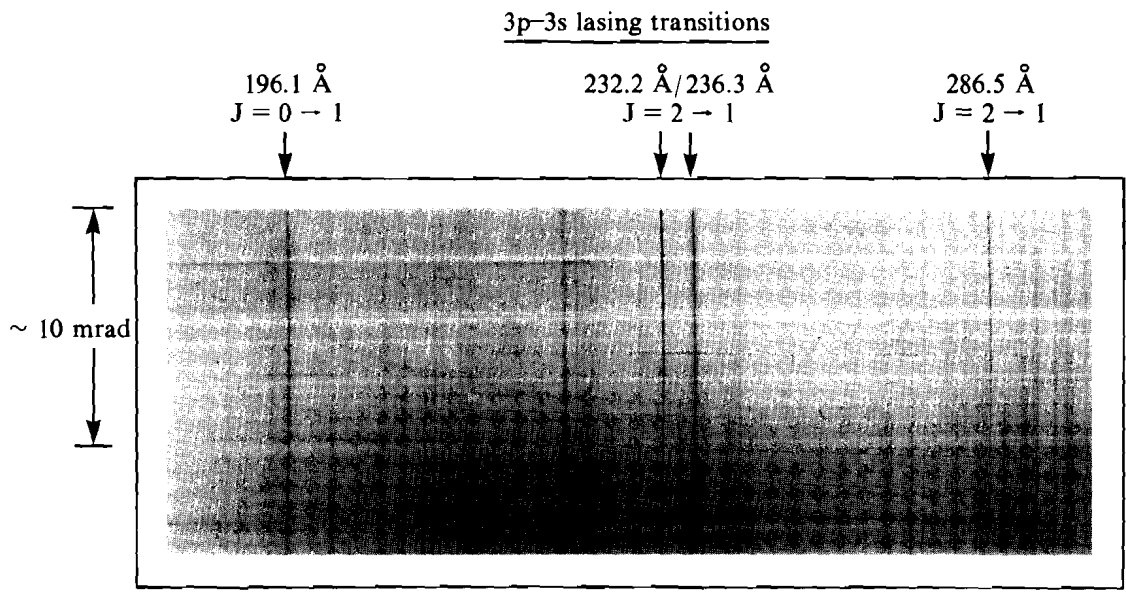
The angular width of the x-ray laser output can be measured using GIGS. Since the output beam of the x-ray laser is of limited extent ($\sim 200 \mu\text{m}$) and narrow ($\sim 10 \text{ mrad}$), the rays fill only a portion of the entrance slit of the spectrometer and are relayed to the film plane as a narrow beam. Providing the acceptance angle of the spectrometer is greater than the x-ray laser divergence, only a limited length of the film is exposed by the lasing line. In contrast, spontaneously emitted x rays are isotropic, fill the slit, and form a spectral line extending across the entire width of the film.

Figure 42.16 is a print of the spectrometer film in the range $\sim 180 \text{ \AA} - 300 \text{ \AA}$. The limited angular extent of the four lasing transitions can be seen in comparison to the nonlasing transitions that fill the spectrometer slit and show no dependence on angle. A measure of the x-ray laser beam divergence can be obtained by plotting the intensity along the spectral line.

The angular peak of the narrow x-ray laser beam is very near the top edge of the spectrometer film. This offset position is a result of the x-ray laser beam refraction by the plasma density profile. This deflection angle is $\sim 10 - 15 \text{ mrad}$ away from the target surface.

The low divergence of the x-ray laser beam makes the measurement of its total intensity difficult. This is a result of the uncertainty as to what portion of the x-ray beam the spectrometer is detecting in the direction perpendicular to the slit. Significant (20%–30%) variation in output intensity for shots of the same length were noted. We believe this is caused by variations in GIGS alignment and shot-to-shot differences in the GDL laser conditions.

Fig. 42.16
A print of the spectrometer film in the region $180 \text{ \AA} - 300 \text{ \AA}$. The variation of intensity along the lasing lines (vertical in photo) represents the angular distribution of the x-ray laser output. Note that the nonlasing lines uniformly fill the width of the spectrometer film.



GDL16786
E5428

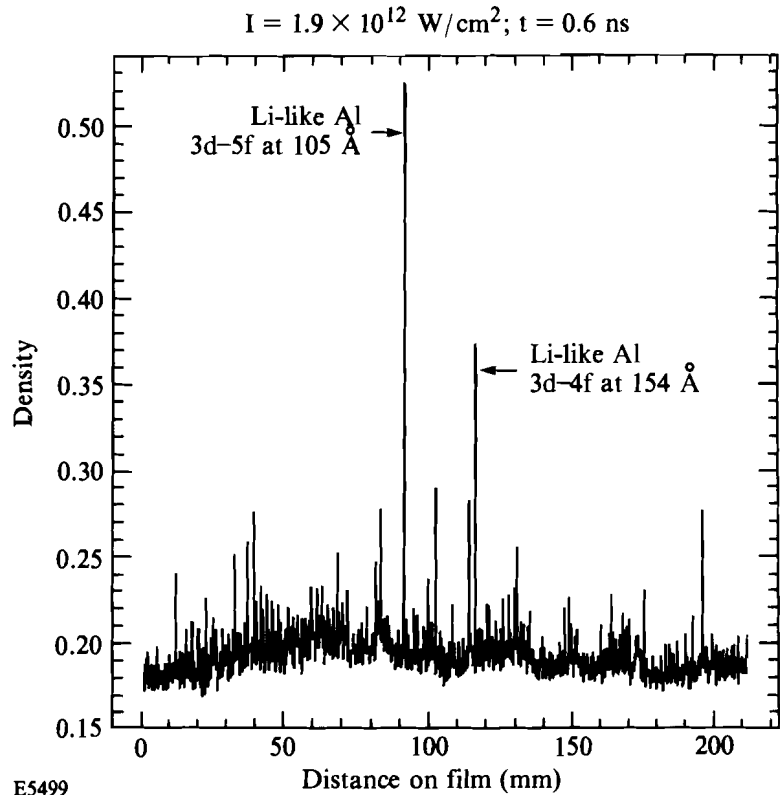
2. Li-like lasing in aluminum and titanium

For the Li-like Al experiments we used the same 650-ps pulse and line focus as described earlier, but reduced the laser energy to about 25 J to give an intensity of 1.9×10^{12} W/cm². The Al targets were constructed out of 125- μ m-thick slabs of aluminum and were mounted as shown in the Fig. 42.12 inset.

Figure 42.17 shows the XUV spectrum from a 14-mm-long Al target. Note that the $3d-5f$ and $3d-4f$ lines of Li-like Al at 105 Å and 154 Å dominate the spectrum, suggesting that these lines have experienced gain. Figure 42.18 shows the intensity (as recorded by GIGS) of the $3d-5f$ line of Li-like Al versus the target length. It also shows that, up to ~14 mm, the line intensity increases exponentially with target length, exhibiting a gain of 2.2 cm⁻¹. For targets longer than 14 mm, the output intensity remains approximately constant, up to 22 mm. The $3d-4f$ line at 154 Å exhibited a similar rollover in the intensity-versus-length curve above 15 mm and exhibited a gain of 2.0 for lengths less than 14 mm. This is possibly the result of refraction that limits the useful length of the plasma. In such a case, the curvature of rays caused by refraction will allow only a 14-mm length of the plasma to contribute to the gain. For lengths greater than 14 mm, the x rays are refracted out of the plasma column before they can sample additional plasma.

Fig. 42.17

The spectrum from a 14-mm-long Al target at an irradiance of 1.9×10^{12} W/cm². Note that the Li-like Al lines at 105 Å and 154 Å dominate the output spectrum for this target.



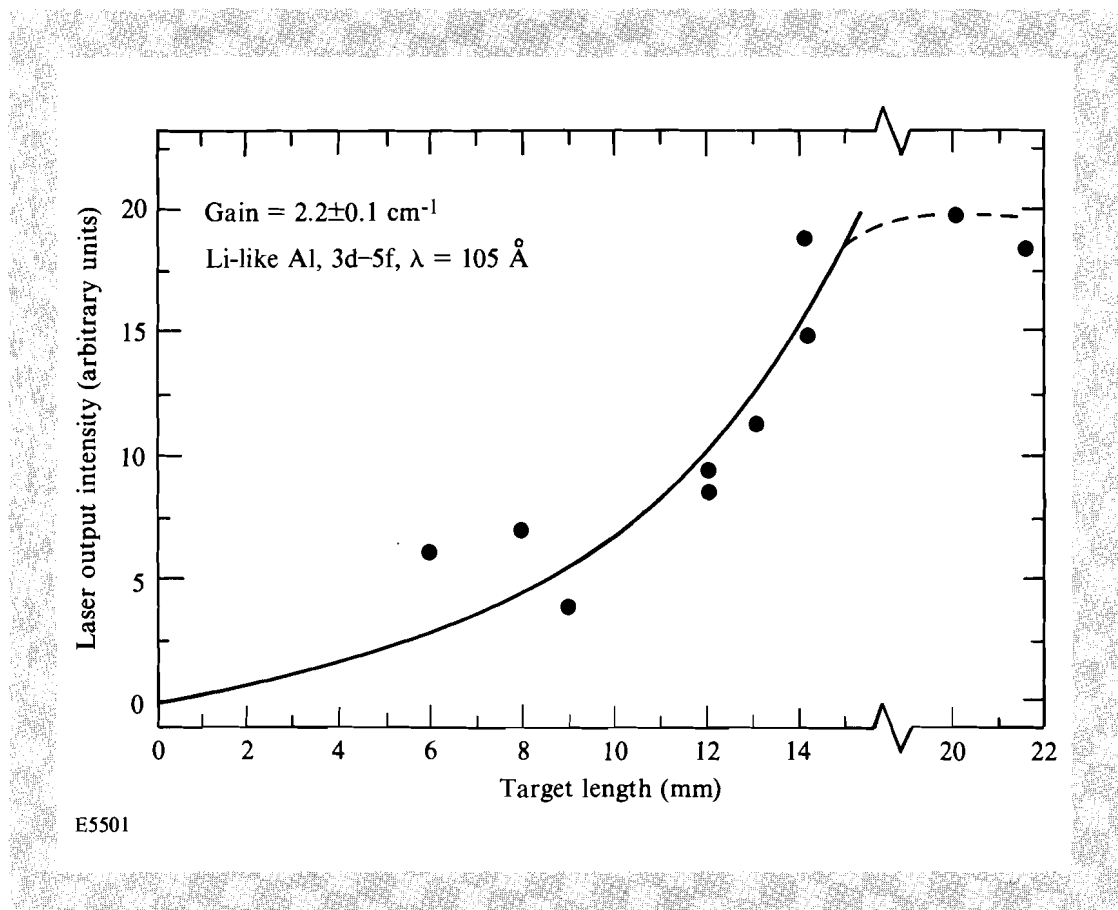


Fig. 42.18

The output intensity of the 3d-5f Li-like Al line at 105 Å for various target lengths. The points are the experimental data and the solid line is a fit of Eq. (1). Note that the line shows exponential growth for lengths less than 14 mm but is nearly constant for longer lengths (dashed curve).

Similar experiments were performed using Ti targets instead of Al. Again, these targets were fabricated out of 125- μm -thick slabs of Ti supported on the standard mount. To obtain the proper ionization (He-like Ti), the laser energy was increased to 200 J, corresponding to an intensity of $1.25 \times 10^{13} \text{ W/cm}^2$. We observed an exponential growth of the 3d-4f line of Li-like Ti at 47 Å for increasing length with a gain coefficient of 2.7 cm^{-1} , as shown in Fig. 42.19.

It should be noted that neither the Li-like Al nor the Li-like Ti lasing transitions exhibited the narrow cone of emission observed for the Ne-like Ge lasers (Fig. 42.16). This may result from lasing occurring at a relatively low density where the gradient is also low (as discussed earlier). A broader region of gain will yield a beam that is broader in angle; therefore, the resulting output of the Li-like x-ray lasers may be broad enough to uniformly fill the spectrometer slit.

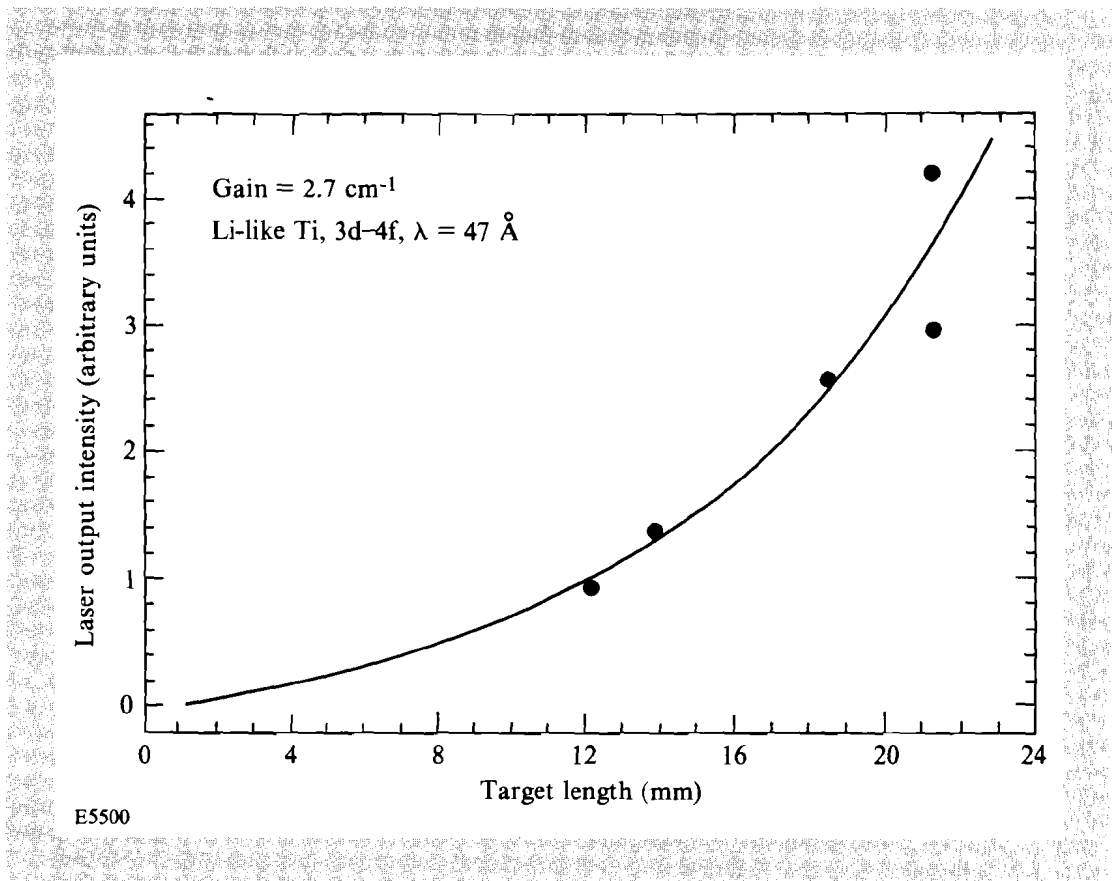
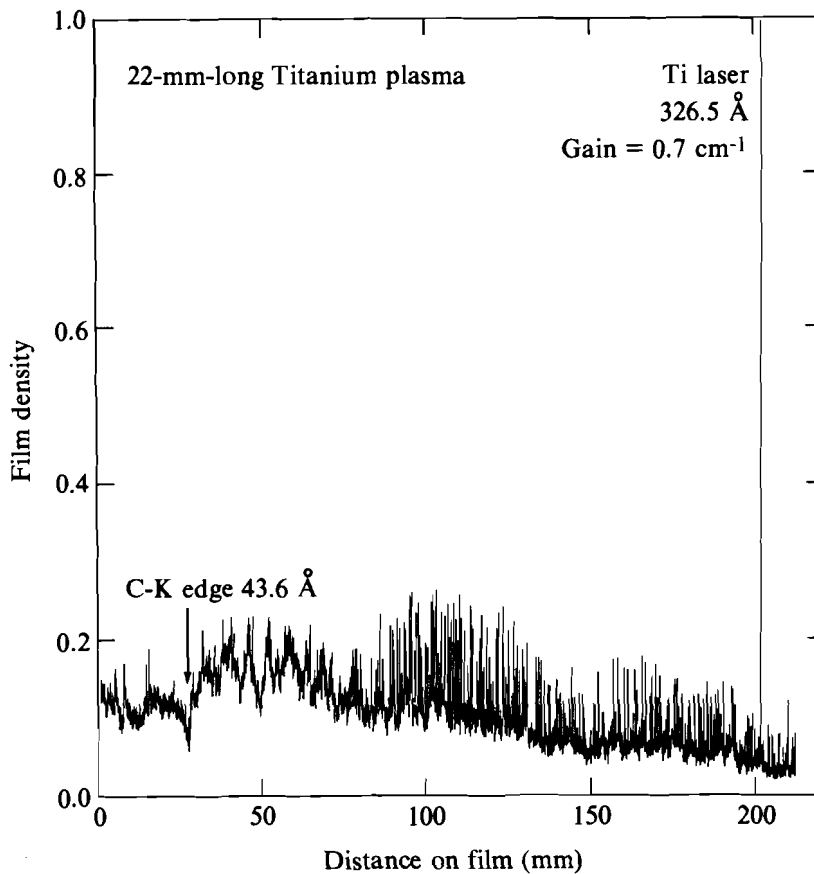


Fig. 42.19

The output intensity of the $3d-4f$ Li-like Ti line at 47 \AA for various target lengths. The points are the experimental data and the solid line is the fit to Eq. (1).

3. Lasing in Ti at 326.5 \AA

At the same irradiation conditions as in the above Ti experiment, an additional line was observed to lase in Ti at 326.5 \AA . This transition is shown in Fig. 42.20, which depicts the GIGS spectrum from a 22-mm-long Ti target. The line at 326.5 \AA is the most intense line in the Ti spectrum, far brighter than the line at 47 \AA in Li-like Ti, which exhibited gain on the same shots. This line has tentatively been identified as a $2p_{1/2}^5 3p_{1/2} (J=0)$ to $2p_{1/2}^5 3s_{1/2} (J=1)$ transition in Ne-like Ti by extrapolating the wavelength values of this transition in various elements.⁷ The other Ne-like lines, which have been observed to lase in other elements ($J=2-1$, $J=0-1$, etc.), lie beyond the current wavelength range of our spectrometer. Figure 42.21 shows the spectrum of a similar shot in the region $10 \text{ \AA}-40 \text{ \AA}$ in which the $n=3$ to 2 lines of Ne-like and F-like Ti are labeled. A group of lines from higher ionization states is also indicated. The presence of both Ne-like and F-like Ti suggests that, at peak intensity, we have ionized the Ti past the Ne-like state and that any lasing in the Ne-like state must occur later as the plasma recombines back into Ne-like. It is still unclear what the pumping mechanism is for the inversion. Besides collisional excitation, it has been suggested that Ne-like lasers can be also pumped by recombination from the F-like ions.² There have also been line coincidences identified by Nilsen¹⁰ that could contribute to the inversion by photo pumping.



E5278

Fig. 42.20

The spectrum from a 22-mm-long Ti target showing the lasing line at 326.5 \AA . This line has been tentatively identified as a $J = 0-1$, $3p-3s$ transition in Ne-like Ti. The $J = 2-1$ lines that lase in Ne-like ions are beyond the range of this spectrometer.

Figure 42.22, a print of the spectrometer film in the range $300 \text{ \AA}-340 \text{ \AA}$, shows the limited transverse extent of the lasing line at 326.5 \AA . A comparison of the angular intensity distribution of one of the Ne-like Ge lasing transitions (236 \AA) and the Ti transition (326 \AA) is shown in Fig. 42.22(a). The Ti laser is about half as divergent as the Ge laser. This difference in divergence may be related to the region where the conditions for lasing are optimal in each case. The Ti laser, having a lower atomic number, will have an optimal density for lasing lower than that of Ge. Moreover, if the Ti laser is driven by other excitation mechanisms, the time at which the two x-ray lasers peak will also be different. Further analysis of the output characteristics of these lasers should reveal the basic manner in which they operate.

The low divergence of the Ti laser allows us to determine the gain in the plasma by comparing the radiation intensity along the axis of the x-ray laser to the emission slightly off axis. The ratio of the intensity I of the ASE (on axis) to the intensity I_0 of the spontaneous emission (off axis) as a function of the gain length ($g\ell$) of the laser is given by

$$I/I_o = [\exp(g\ell) - 1]/(g\ell). \quad (2)$$

From this relation we determine the gain coefficient of the 326.5-Å Ti laser to be 2.7 cm^{-1} for a length of 22 mm.

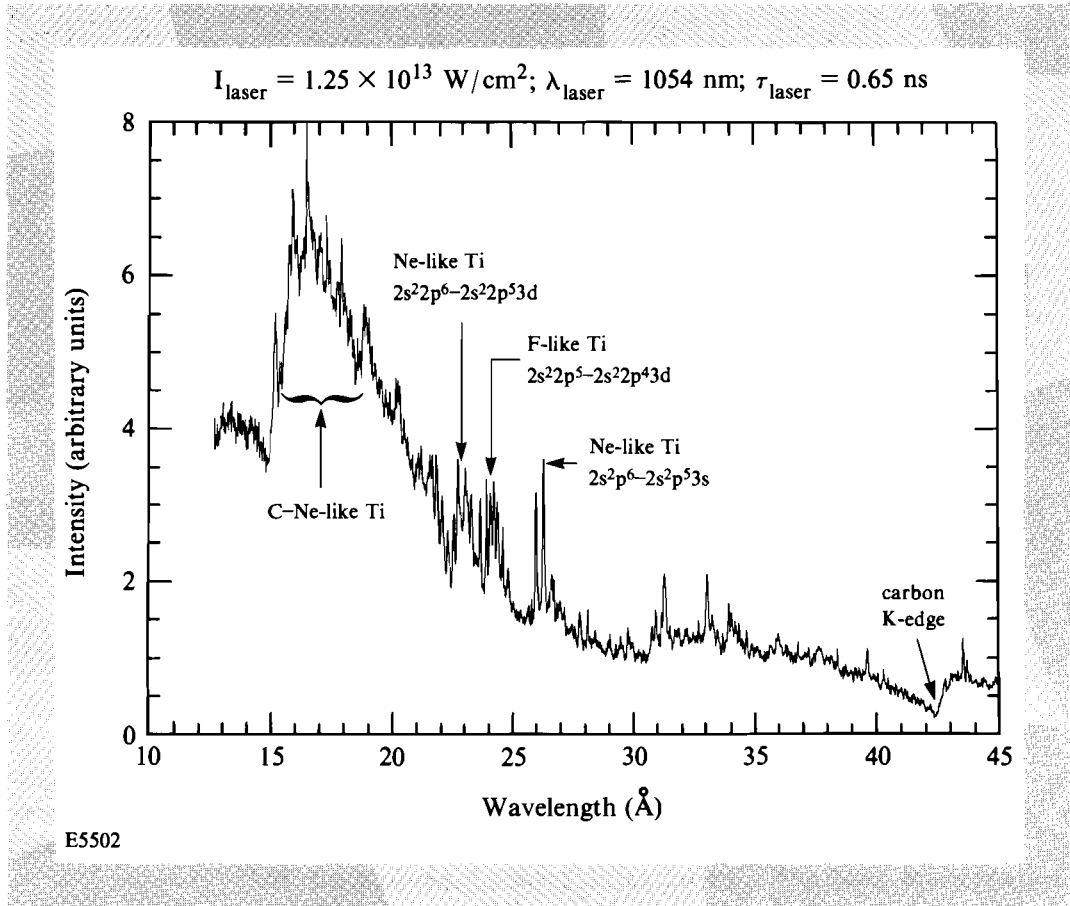


Fig. 42.21

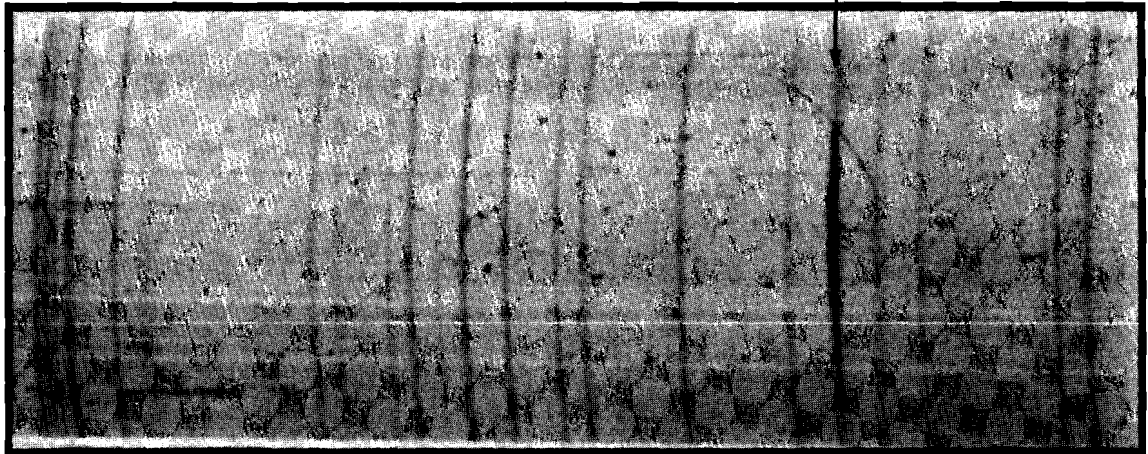
The spectrum from a 22-mm-long Ti target. This spectral region (10 Å–40 Å) contains the $n = 3$ to $n = 2$ lines of Ne-like and F-like Ti. The presence of Ne-like emission supports the claim that the lasing line at 326.5 Å is from Ne-like Ti.

Summary

We have demonstrated several types of lasing using slab targets. We observed gains in the range of 1.0 to 2.5 cm^{-1} in the various $3s-3p$ Ne-like Ge transitions previously observed in both exploding-foil targets and slab target geometries. These results were obtained using the lowest optical laser energies reported to date. Our results include a measurement of the angular divergence of the x-ray laser beam in one dimension.

We have also observed gain on the $3d-5f$ and $3d-4f$ transitions in Li-like Al at 105 Å ($g = 2.2 \text{ cm}^{-1}$) and at 154 Å ($g = 2.0$), respectively. These transitions have previously been observed at lower irradiances with longer

Lasing line of Ti^{+12} at 326.5 \AA shows $\sim 4\text{-mrad}$ divergence.



GDL16837
E5281

Fig. 42.22

A print of the spectrometer film in the region of the Ti lasing transition at 326.5 \AA . The narrow angular extent of the x-ray laser output can be readily seen (see also Fig. 42.16). Both the ASE (on axis) and the unamplified spontaneous emission can be measured from this spectrum.

pulse widths. Our results extend the range of laser conditions for which these transitions have been observed to lase. We also extended this scheme to a relatively short wavelength, 47 \AA , by demonstrating a gain of 2.7 cm^{-1} on the $3d\text{-}4f$ Li-like transition in Ti.

The Li-like lasing transitions (in Al and Ti) appear to behave differently than Ne-like lasers in that no angular distribution peak could be discerned in the output intensity. As the gain medium in an x-ray laser increases, the output beam is dominated by the few rays that experience the most gain. Typically these rays are limited in direction and cause the output beam to get narrower as the medium gets longer. The lack of measured directionality may result from the recombinationally pumped lasers experiencing gain in an extended region of the plasma where more than one path exists through which rays can experience gain. If these multiple paths contain equivalent gain, a wider output beam would be produced. The fact that the output of the Li-like Al emission does not continue to grow exponentially with lengths greater than $\sim 14 \text{ mm}$ also suggests that no localized collection of rays has begun to dominate the output.

Originally it was thought that a slab target could not produce gain because steep density gradients would refract the x rays out of the plasma before significant path length is achieved. Therefore, it is important to understand

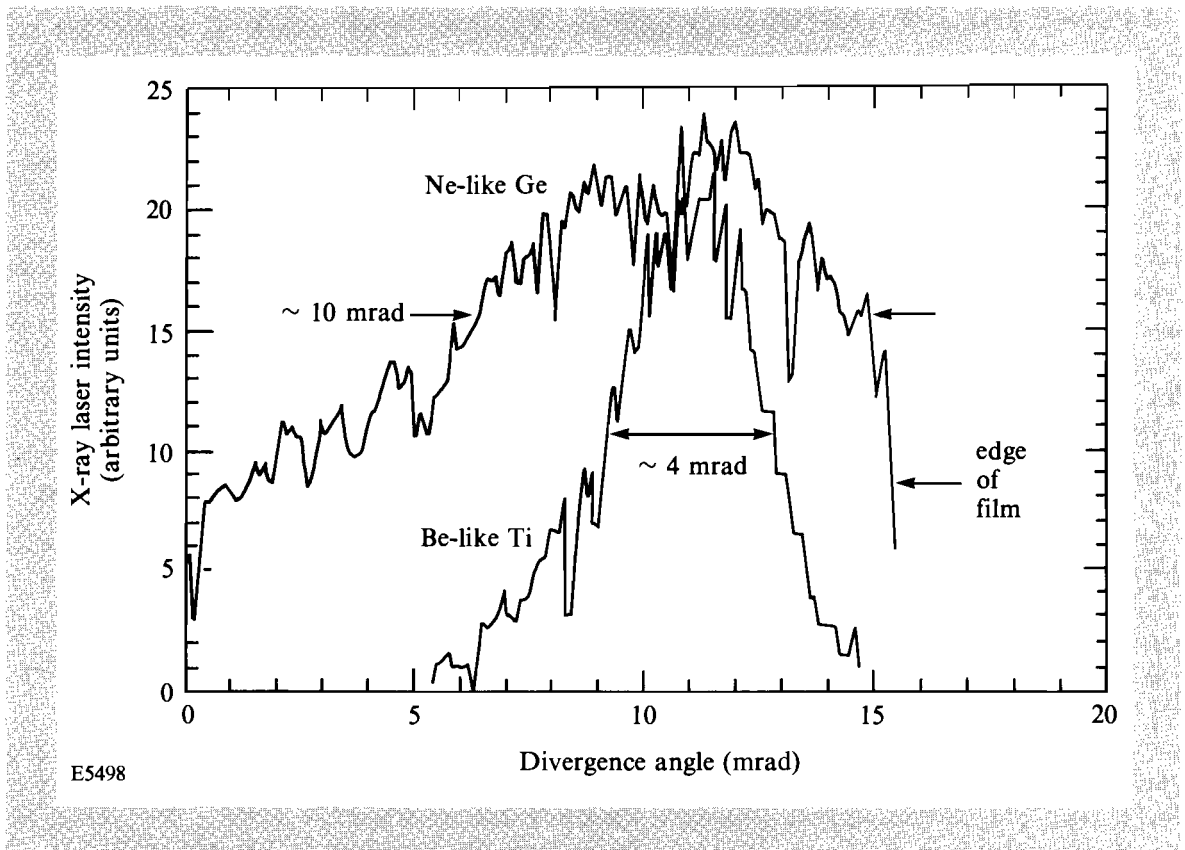


Fig. 42.22(a)

A comparison of the angular intensity distributions of the Ne-like Ge laser (236 Å) and the Ti laser (326 Å).

how these slab-target x-ray lasers behave. We have developed both analytical¹¹ and numerical¹² models that treat the refraction of x-ray laser beams in various types of targets. These models should help us explain where the x rays experience most gain and how they propagate through the target. The numerical code solves the three-dimensional ray-trajectory equation through the two-dimensional density profiles generated by a separate hydrocode. The local gain (as a function of temperature and density) has been calculated using a detailed atomic physics code.¹³ By following various rays through the plasma, applying the calculated gain, and summing their contributions we will be able to compare the predictions to the experiments and comment on the relative importance of refraction in various target types.

Finally, we have observed a gain of 2.7 cm^{-1} on a transition at 326.5 Å in Ti. We will attempt to identify this transition by extending the range of the GIGS to include the other predicted Ne-like lasing transitions. If this transition is indeed Ne-like, then there are a number of additional questions to be resolved. For example, the gain is higher than predicted by the scaling of gain in Ne-like ions with atomic number as demonstrated by Lee

et al.,³ from which an extrapolation to Ti results in a gain of nearly zero. This suggests that there may be pumping mechanisms other than collisions that contribute to gain in the Ti x-ray laser.

ACKNOWLEDGMENT

This work was supported by the Naval Research Laboratory under contract N00014-86-C-2281 and by the Laser Fusion Feasibility Project at the Laboratory for Laser Energetics, which has the following sponsors: Empire State Electric Energy Research Corporation, New York State Energy Research and Development Authority, Ontario Hydro, and the University of Rochester.

REFERENCES

1. D. L. Matthews *et al.*, *Phys. Rev. Lett.* **54**, 110 (1985).
2. C. J. Keane *et al.*, *J. Phys. B.* **22**, 3343 (1989); R. A. London *et al.*, *ibid.* **22**, 3363 (1989).
3. T. N. Lee, E. A. Mclean, and R. C. Elton, *Phys. Rev. Lett.* **59**, 1185 (1987).
4. D. Kim *et al.*, *J. Opt. Soc. Am. B* **6**, 115 (1989).
5. P. Jaegle *et al.*, *J. Opt. Soc. Am. B* **4**, 563 (1987); G. J. Pert, *Plasma Phys. & Controlled Fusion* **27**, 1427 (1985); S. Suckewer *et al.*, *Phys. Rev. Lett.* **55**, 1753 (1985); J. F. Seely, C. M. Brown, U. Feldman, M. Richardson, B. Yaakobi, and W. E. Behring, *Opt. Commun.* **54**, 289 (1985); P. R. Herman *et al.*, *IEEE Trans. Plasma Sci.* **16**, 520 (1988).
6. T. Hara *et al.*, *Proc. Japan. Acad.* **65**, 60 (1989).
7. J. H. Scofield (private communication).
8. W. Seka, J. M. Soures, S. D. Jacobs, L. D. Lund, and R. S. Craxton, *IEEE J. Quantum Electron.* **QE-17**, 1689 (1981).
9. B. L. Henke *et al.*, *J. Opt. Soc. Am. B* **1**, 818 (1984); B. L. Henke *et al.*, *ibid.* **1**, 828 (1984).
10. J. Nilsen (private communication).
11. B. Boswell, D. Shvarts, T. Boehly, and B. Yaakobi, to be published in *Phys. Fluids B*.
12. R. S. Craxton, 10th Annual Anomalous Absorption Conference, Durango, CO, 19–23 June 1989; also R. S. Craxton, *LLE Review* **38**, 88 (1989).
13. M. Klapisch, *Comput. Phys. Commun.* **2**, 239 (1971).